The International Journal of Advanced Manufacturing Technology (2022) 119:149–161
https://doi.org/10.1007/s00170-021-08110-2

ORIGINAL ARTICLE

Design and analysis of compound structures integrated with bio-based phase change materials and lattices obtained through additive manufacturing

Daniele Almonti[1] · Emanuele Mingione[2] · Vincenzo Tagliaferri[1,3] · Nadia Ucciardello[1]

Received: 2 August 2021 / Accepted: 20 September 2021 / Published online: 25 October 2021

Abstract
Phase change materials (PCMs) are an interesting category of materials employed in latent heat thermal energy storage, such as ad hoc designed heat exchangers. Nowadays, there are several typologies of PCMs, which derive from the wastes of the agricultural industry, which could be used for this kind of design. Each material made of biological waste has a different melting/solidification point and latent heat of fusion/solidification, which means flexibility of design on the heat exchangers by considering the different thermal proprieties of the chosen material. Also, using recycled material from wastes can lead to an overall improvement of the resources and goes hand in hand with the need of today's society to aim more and more at a Circular Economy. The industrial development of this kind of material is limited by its thermal properties, such as poor thermal conductivity both in liquid and solid phases, leading to low heat transfer effectiveness. To overcome these limitations, in this paper, the bio-based PCMs were integrated into a metallic reticular structure made of copper and aluminium and realised through Indirect-Additive Manufacturing, to improve the overall thermal conductivity of the system and increase the efficiency of the heat transfer. Four compound structures filled each time with four different PCMs were realised and tested, in order to thermally characterise each combination of materials used and choose which one has an overall better thermal behaviour. The results showed how the thermal storage/release was improved by 10% for the copper reticular structure, even if must be considered the tradeoff between better thermal management and the increase of the costs and the weight of the designed heat exchanger.

Keywords PCM · Additive manufacturing · Heat exchangers · Thermal storage · Circular economy

1 Introduction

The increase in energy demand and environmental issues due to the widespread use of fossil fuels encouraged many countries to focus on sustainability, for this reason, renewable and sustainable energy sources are getting more and more important [1–3]. One of the most affordable and favourable sources of renewable green energy which is drawing particular attention is the solar one [4, 5]. During the last decades, researchers in different areas of study have tried to improve the efficiency of energy production systems through solar sources. The included researches concerned the enhancement of the heat transfer process during the storage [6–9], upgrading the solar technology photoresponsivity [10, 11], and the usage of high-performance materials [12–14]. In optic of an overall increase of the performance of solar energy in general, storage systems must be considered. Storage of energy could occur as latent heat during the transition of material phases at specific temperatures, i.e. liquid to solid.

A family of materials used for solar energy storage are known as phase change materials or briefly PCMs. Compared with usual heat storage systems in PCMs a larger quantity of energy can be stored in smaller weights and volumes due to the phase transition. Also, during the charging and discharging of energy, there are smaller temperature

✉ Emanuele Mingione
emanuele.mingione@unicampania.it

[1] Department of Enterprise Engineering, University of Rome Tor Vergata, Via del Politecnico 1, 00133 Rome, Italy

[2] Department of Engineering, University of Campania Luigi Vanvitelli, Via Roma 29, 81031 Aversa, CE, Italy

[3] CIRTIBS Research Centre, University of Naples Federico II, P.le Tecchio 80, 80125 Naples, Italy

differences than other conventional sensible heat storage media because of the small temperature swing, which leads to an increased versatility in various applications. For these reasons, PCMs could be implemented in small-size systems [15–17]. The implementation of PCMs in industrial applications involves the charging or discharging of the material with a specific amount of thermal energy by having heat transfer with working fluids. However, the low thermal conductivity of the PCMs is the main drawback since it lowers the overall efficiency of the thermal systems. Consequently, an increment in the thermal conductivity and heat transfer of a PCM package is the key factor for using them on a wider range of industrial applications. Many research projects have been conducted to increase the effective surface area of the package, to enhance the thermal charging and discharging [18]. Cao et al. [19] reported that the PCM melting rate is accelerated by adding fins to the structure which contains it. In the work is defined a time-averaged Nusselt number which considers the efficiency of the heat transfer mechanism. By implementing the time-averaged Nusselt number, they found out that with an increment of the number of fins, the area of the heat transfer surface is increased whilst the heat transfer coefficient is decreased. The number of fins is a key factor for the improvement of conductive wall heat transfer. Joneidi et al. [20] made an experimental study to evaluate the melting phenomenon in a horizontal heat sink with plate fins by changing the height and the number of fins. Their results showed that adding fins to the enclosure leads to a lower base temperature and a higher melting rate. In particular, a more uniform temperature distribution is achieved by increasing the number of fins. Also, they found that the number of fins has a more significant effect if they are below the critical temperature. Adem et al. [21] performed an experimental study and added fins to the PCM enclosure. They found that although adding fins can decrease the melting time of PCM, an increment in the fins' thickness can cause adverse effects on the melting time.

Together with industry, another one of the main sectors of energy consumption and environmental pollutions in the world is buildings since it is one of the most responsible energy consumption sectors [22]. It is stated by various researchers that the energy consumption in buildings accounts for 20 to 40% of the total energy usage depending on location, and 36% of CO_2 emissions are sourced by buildings in Europe [23–25]. At this point, the reduction of energy consumption of buildings has gained special attention for the sustainability of the habitats of society that mainly consist of buildings [26]. Therefore, researchers focus on the studies that consider various ways for energy and emission reduction of buildings, which contributes to sustainable solutions and thermally more comfortable living places [27, 28]. Other than the classic produced PCMs (Paraffin 32, Lauric Acid, Petroleum Jelly, Capric Acid, Vaseline, etc.) the ones manufactured by bio-based components from agricultural wastes are particularly interesting in optic to increase the overall efficiency of the entire production process and achieve the aims of the Circular Economy and recycle of the industrial wastes.

In this paper, 4 bio-based PCMs derived from agricultural wastes (Pure Temp 68, Crodatherm 60, Crodatherm 74, Crodatherm ME29P) were thermally tested and characterised. All the aforementioned PCMs were chosen since they are awarded with many Sustainable Development Goals (SDG) from SDG 12 to SDG 15, which ensures the 0% environmental impact of the adopted materials. To overcome the limitations of the PCMs (low thermal conductivity both in liquid and solid phases) the bio-based materials were integrated with metallic reticular structure realised through I-AM. The novelty of this combination consists of the creation of a monolithic metallic structure without needing to join the internal reticular structure to the external pipe. The entire structure is realised through the 3D printing of the resin model and the subsequent investment casting of the metal, which can be filled with the PCM with a high surface/volume ratio, enhancing the thermal exchange since there is better continuity of the material. Those goals could not be reached with conventional technologies. Other unconventional technologies that can be used for the production of metallic samples can be the AM through EBM or SLM. The disadvantages of those processes compared to the stereolithography are the higher presence of air entrapment, which leads to an overall lower thermal behaviour, and higher production costs of the machinery used for the modular realisation of the samples. Almonti et al. [29–31] used stereolithography 3D printing to produce foam models made of a foundry resin. Following, this model was reproduced with a casting process to achieve a metal foam with the designed structure. The compound structures analysed in this work were produced with the aforementioned bibliography methodology and made of aluminium AC-44300 and copper alloy, with two different pore dimensions (Ø 3.2; Ø 6.4). The chosen PCMs typology were melted and integrated into the reticular structures. The differences between each of the 16 configurations analysed were evaluated through thermal imaging. Moreover, for each sample were evaluated the power absorbed and released expressed in terms of unit length (respectively P_{tot}^{h*} and P_{tot}^{c*}) for a better comparison of the results, since the produced structures can be part of a modular system projected ad hoc for solar thermal storage.

The conceptualization of the modular system follows the guidelines established by Bi et al. [32] and is showed in Fig. 1. Different modulus filled with bio-based material can be connected and integrated into solar panels, to accumulate the heat necessary for the phase change of the PCM, which can work as a heat exchanger and distribute the absorbed

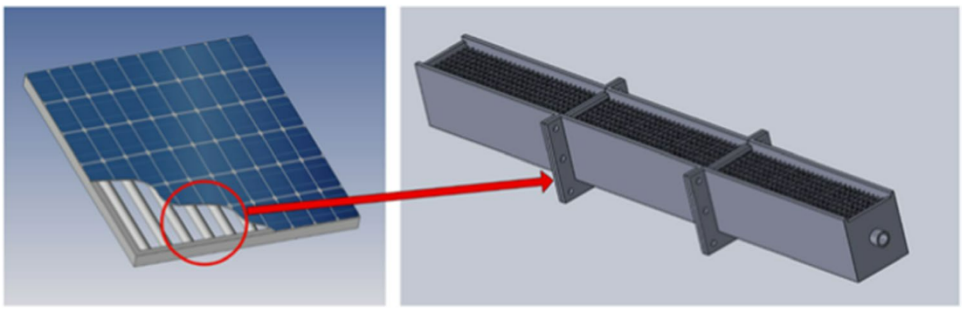

Fig. 1 Conceptualization of the modular system which can be integrated in solar panels for the storage of thermal energy

energy for different applications (i.e. the production of hot sanitary water for domestic use).

Finally, an ANalysis of VAriance (ANoVA) was performed. In literature, ANoVA is used to understand the significant factors in experimental results [33–35]. In the present work, it was applied to evaluate the influence of the PCM and structural parameters during both the heating and cooling phase of the experimental tests.

2 Materials and methods

Reticular structure models were designed by means of the CAD software Solidworks. Initially, the 2D with the external pipes and the reticular configuration were drawn. Therefore, the sketch was extruded along *Z* axis for 40 mm, obtaining the final reticular structure configuration shown in Fig. 2.

After the CAD realisation, the resin models were realised through the stereolithography 3D printer XFAB 2000 DWS with a photosensitive resin FUSIA 444. The internal reticular structure of the pipes allows obtaining the printing process without external supports. Following, the realised compound structures were polymerized for 1 h in a UV oven. Following the realisation phase, the resin models were analysed and measured through a system of optical microscopy HIROX-RH-2000 and 3D laser scanner ZG Technologies – Atlascan to check the conformity to the specifics of the realised models. After the realisation of the resin model, it was made the plaster mold necessary for the direct casting. Plaster suspension was produced by mixing plaster powder and water at 25 °C for 4 h. In order to eliminate air inclusions in the suspension and prevent defects during the casting process, a vibrating platform and a vacuum machine were used. Successively, the suspension was inserted in the foundry cylinder to form the plaster mold. A thermal cycle was imposed on the plaster mold to remove the resin, consolidate its structure and reach the casting temperature. After, the casting process was made through the foundry machine ASEG Galloni G5 that enable the metal to melt in an inert atmosphere (Argon). Those phases are specular for both copper and aluminium samples. Subsequently, the molten metal fills the mold through a vacuum. Following the casting process, the plaster was removed from the cylinder after 6 h of cooling. The samples realised through the entire process of I-AM are shown in Fig. 3.

Once the realisation phase is over, it proceeded with the filling of the compound structures. Four typologies of bio-based PCM fillers were studied, adopted, and characterised. The thermal properties of the fillers are described in Table 1.

During the filling phase, for each sample it was turned an Aluminium base with an o-ring housing seat in the internal part, where subsequently was inserted a gasket, to avoid the

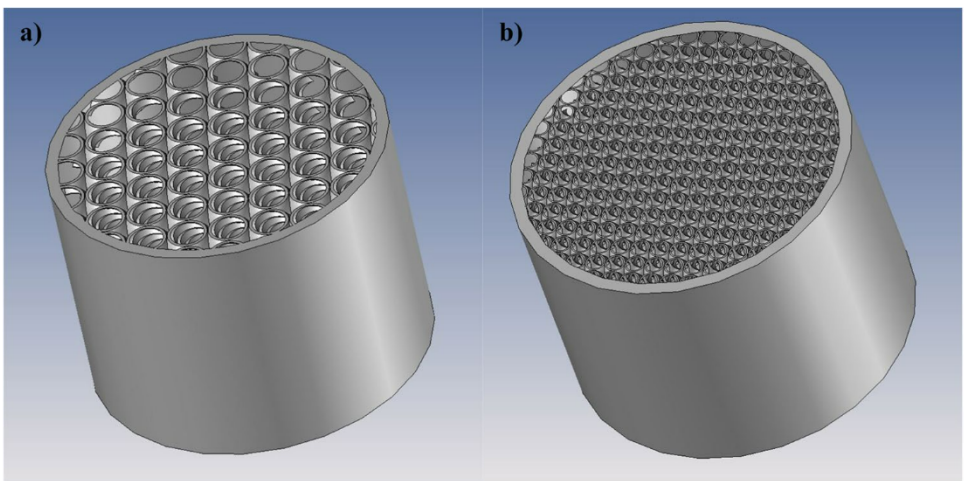

Fig. 2 CAD of the reticular structure models: **a** Ø 6.4; **b** Ø 3.2

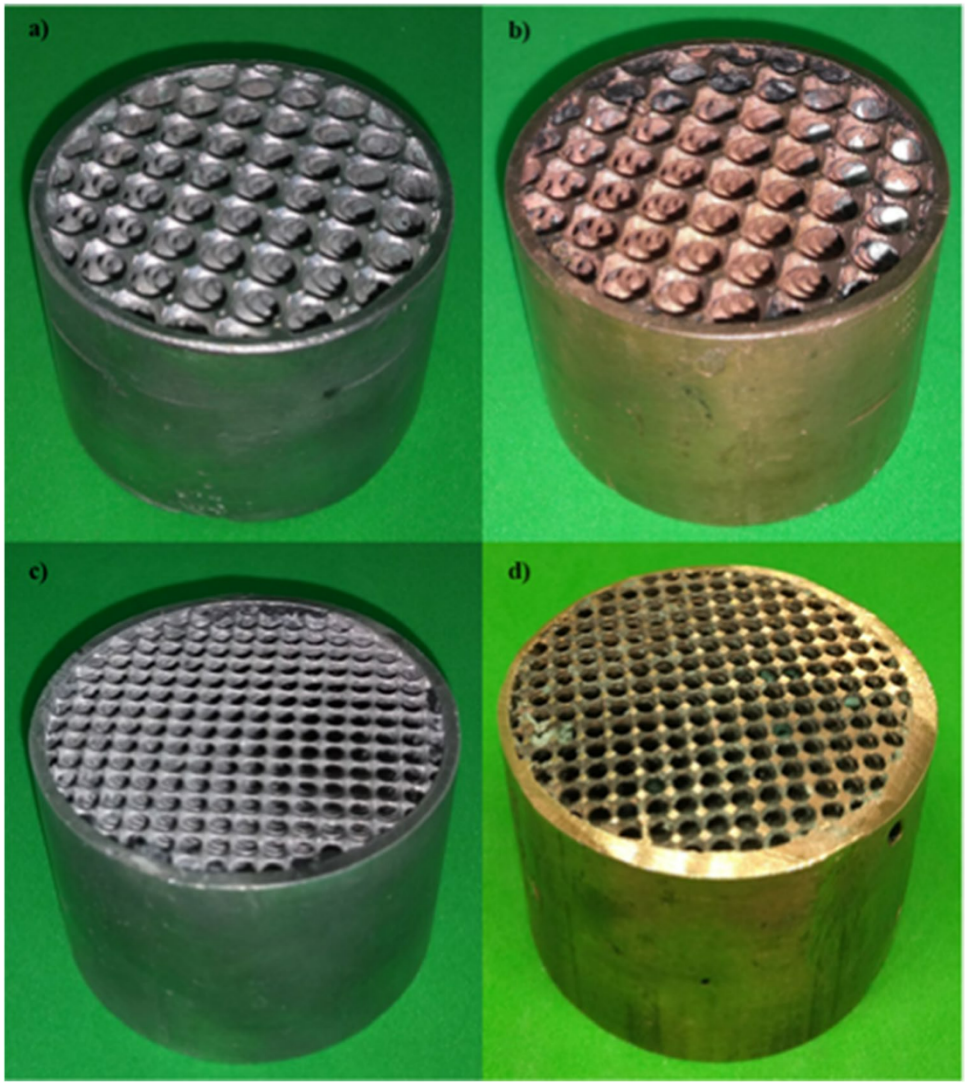

Fig. 3 Reticular structure realised through I-AM: **a** Aluminium Ø 6.4; **b** *Copper* Ø 6.4; **c** Aluminium Ø 3.2 **d** Copper Ø 3.2

Table 1 Thermal properties of the bio-based PCM fillers analysed

	Pure Temp 68	Crodatherm 60	Crodatherm 74	Crodatherm ME29P
Melting point [°C]	68	59.8	74.8	28.8
Latent heat (melting) [J/g]	213	217	226	183
Latent heat (solidification) [J/g]	− 213	− 212	− 224	− 179
Specific heat (liquid) [J/g°C]	1.91	1.4	1.8	1.4
Specific heat (solid) [J/g°C]	1.85	2.3	2	2.3

leaking of the liquid PCM filler. However, this solution was not effective since the gasket alone was not enough for sealing the liquid. This problem was solved by adding a vacuum bag sealant through the gap between the sample and the aluminium base, giving additional protection from the leaking of the PCM in the liquid phase. Once achieved the bases for each metal sample, each typology of bio-based filler was heated up at its melting temperature, and successively it was versed into the reticular structures realised. The filled compound structures were left cooling for 3 h at environmental temperature (25 °C) to let the PCM filler solidify inside the reticular samples. Since there was an excess of bio-based material, a mechanical cleaning showed in Fig. 4 was needed after the filling phase, to obtain the final tested structures.

After the filling phase, the experimental tests were carried out. Samples were enveloped with a 1 m linear

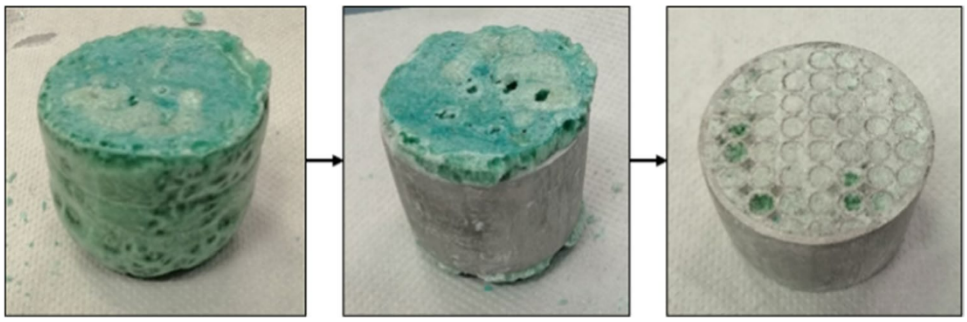

Fig. 4 Sample in different phases of the mechanical cleaning after the filling phase

resistance (30 W/m) with 6 spires in total, to heat the samples in a controlled way. The experimental setup to analyse the thermal performance of each PCM is shown in Fig. 5. Each sample filled with the PCM filler enveloped with the linear resistance on the aluminium base was connected to a controller which heats the system until it reaches the desired working temperature (80 °C). To control the temperature during the heating phase, a thermocouple type K was inserted at the centre of the reticular structure. Once the thermocouple measures a $T > 80$ °C the controller turns off and stops providing electric power to heat the sample. The working temperature of 80 °C was chosen since is higher than the temperature of transition in the liquid phase for every typology of PCM filler considered.

The single test has been structured in different steps:

1. During the first step, the controller is turned on, providing thermal power (30 W) for conduction on the lateral surface of the sample for 40 min. The PCM filler during this step will change its phase, turning from solid into the liquid phase.
2. During the second step, the controller is turned off, and the cooling happens by natural convection at environment temperature (~ 20 °C) for 80 min. During this step, the PCM filler will change again its phase turning from a liquid into a solid phase.

The duration of the test is 120 min. The entire temperature field is evaluated through a thermal camera FLIR A655sc with lens Close-up 2.9 × (50 µm), connected to the respective software for digital thermography analysis. As shown in Fig. 6 in each test were extracted 7 temperature histories from the core points (cursor) defined as follows:

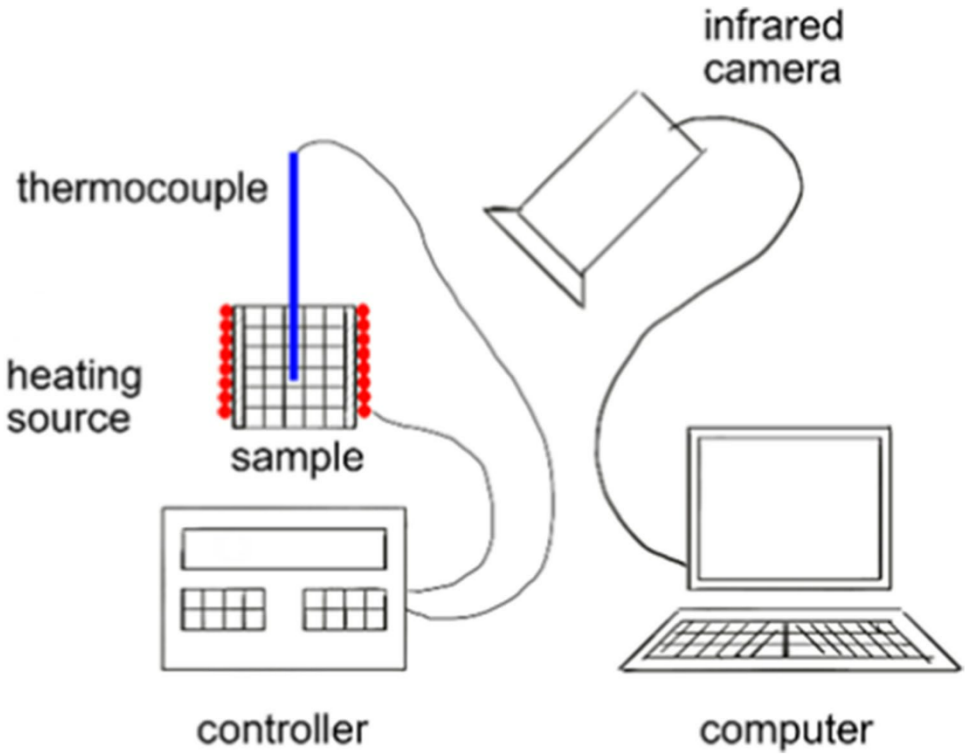

Fig. 5 Experimental setup used to evaluate the thermal performance of the PCM fillers integrated into the reticular structures

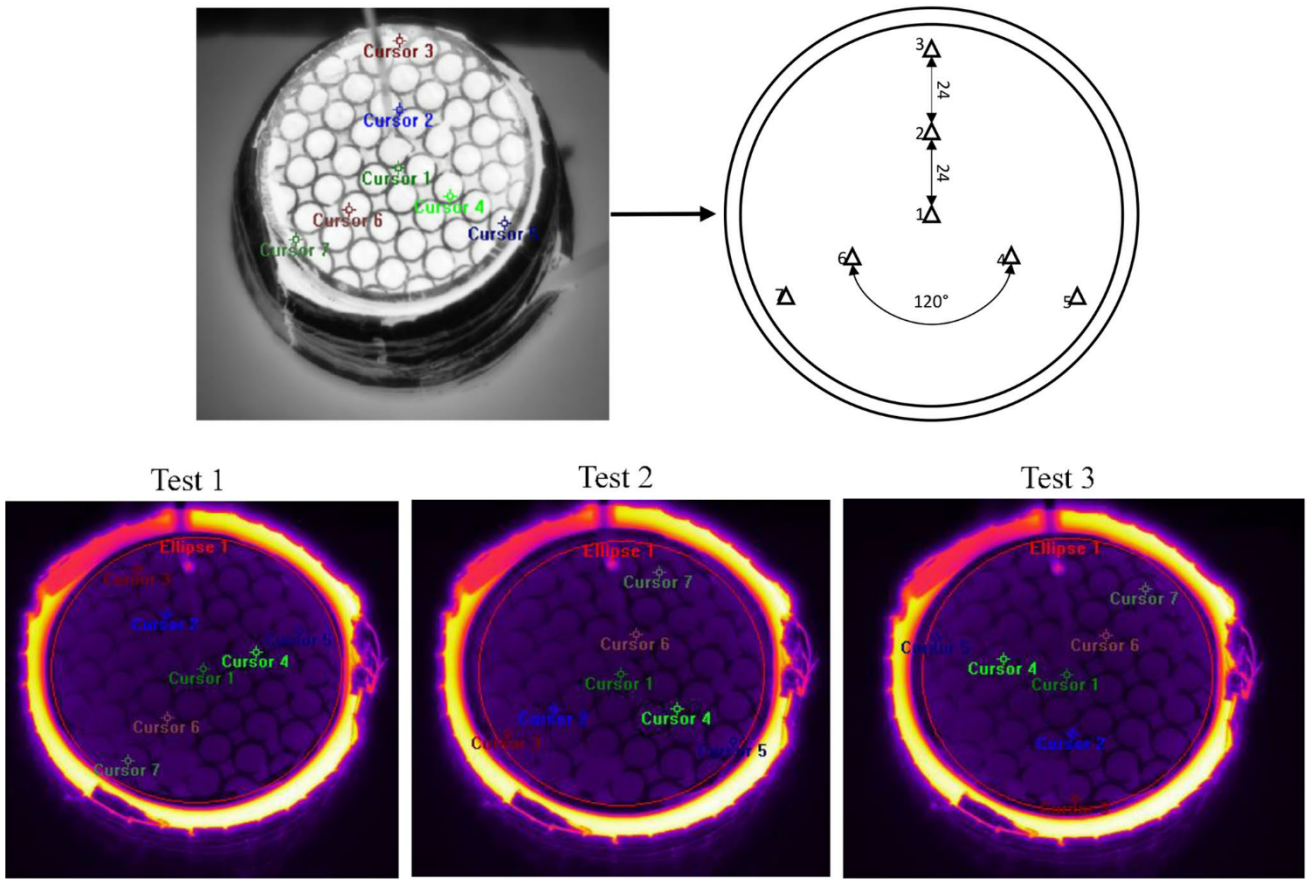

Fig. 6 Schematic and effective representation of the point of interest (cursor) for each repeated test

- Cursor 1: based in the middle of the section of the sample;
- Cursor 2–4–6: based on the circumference of medium-range from the section;
- Cursor 3–5–7: based in proximity of the maximum ray circumference in the section.

Each copper and aluminium sample was filled and tested with each PCM filler considered for this study, so a total of 16 different structures (4 × 4) were performed. Also, each structure was tested 3 times, and the cursor position during each test was changed by rotating them by 90°, to verify the repeatability of the temperature history results. A total of 48 experiments were performed.

In order to compare the different reticular structures, the materials and the PCM fillers, an analysis of the thermal power for unit length absorbed and ceded during the tests. Were evaluated from the mean temperature histories the following parameters:

- The max Temperature during the heating phase (T^h) is considered as the max temperature reached before the first oscillation due to the shutting down of the controller
- The environmental Temperature (T_{start})
- The temperature of start cooling (T^c) is considered as the max temperature reached during the last oscillation before the shutting down of the controller
- The temperature of end cooling (T_{end}) is considered as the temperature measured at the end of the testing
- The heating time (t_h) is considered as the time spent by the controller to reach the max Temperature during the heating phase (T_h)
- The cooling time (t_c) is considered constant of 80 min which is the time where the controller is turned off until the end of the measurement phase which happens by convection cooling.

Besides the known quantities obtained by the results from thermography, and known respectively:

- The mass of the sample without filler (m_v)
- The mass of the PCM filler inside each reticular structure (m_f)
- The latent heat of fusion and solidification of the PCM typology analysed (λ_s, λ_f)
- The solid and liquid specific heat of the PCM fillers (c_s, c_l)

- The specific heat of the copper and aluminium (c_m)
- The temperature of the transition phase of the PCM (T_{tf})
- The length of the 3D printed reticular structures (L)

It was possible to evaluate the heating absorbed/ceded from the PCM fillers during the heating/cooling phases by means of the Eqs. (1, 2).

$$Q^h = \left[m_f \times c_s \times \left(T_{tf} - T_{start}\right)\right] + \left(m_f \times \lambda_f\right) + \left[m_f \times c_l \times \left(T^h - T_{tf}\right)\right], \tag{1}$$

$$Q^c = \left[m_f \times c_l \times \left(T^c - T_{tf}\right)\right] + \left(m_f \times \lambda_s\right) + \left[m_f \times c_s \times \left(T_{tf} - T_{end}\right)\right]. \tag{2}$$

By defining the specific heath of the metals used (copper/aluminium) it is possible to calculate in the same way the heating absorbed/ceded from the reticular structure by means of the Eqs. (3, 4).

$$Q_m^h = m_v \times c_m \times \left(T^h - T_{start}\right), \tag{3}$$

$$Q_m^c = m_v \times c_m \times \left(T^c - T_{end}\right). \tag{4}$$

With c_m that is respectively 0.88 J/g°C for aluminium reticular structure, and 0.39 J/g°C for the copper reticular structure. Successively, it was calculated the power absorbed/ceded by merging the contributes of the PCM filler and the reticular structure, and dividing the contributes for the different times of each phase (5, 6).

$$P_{tot}^h = \frac{\left(Q^h + Q_m^h\right)}{t^h}, \tag{5}$$

$$P_{tot}^c = \frac{\left(Q^c + Q_m^c\right)}{t^c}. \tag{6}$$

Moreover, considering the possible differences of length in the 3D printed reticular structures, they were measured with calibre and were evaluated the power expressed in terms of unit length of each sample by dividing the, respectively, total power during the heating/cooling phase for the length of the samples (7, 8).

$$P_{tot}^{h*} = \frac{P_{tot}^h}{L}, \tag{7}$$

$$P_{tot}^{c*} = \frac{P_{tot}^c}{L}. \tag{8}$$

3 Results

The realised resin models were analysed and measured through a system of optical microscopy HIROX RH2000 and 3D laser scanner ZG Technology—Atlascan. The comparison between CAD models and resin printed components shows a difference of 0.2–0.5 mm on diameter and axial length, whilst the differences slightly decrease for the smallest parts, such as the thickness of the ligaments and the diameters of the holes (0.01–0.05 mm). These results are in accordance with tolerances generated by the SLA process considering the influence of the laser spot on photopolymerization. Beyond the normal optical imaging, were also made tiling and multi-focus measurements with rotating angular optics. The data were successively elaborated through the microscopy software HIROX and shown in Fig. 7 and Table 2.

In Table 3 were reported the weights of the as-built samples realised and every PCM filler typology analysed, to calculate subsequently the heat absorbed and transmitted during the testing phase. From the table, it can be observed that all the weight of each metallic structure realised differs by less than 2% from the ones calculated numerically via CAD by knowing the volume and the density of the materials. The weight of the PCM in each reticular structure was calculated by subtracting the weight of the as-built sample and the aluminium base from the filled structures.

Microscopical observation of the filled samples showed in Fig. 8, underlines that PCM coexists without discards with the metal matrix. This coexistence is an extremely favourable feature in the management of thermal energy. The filler evens the heat distribution both in the heating and cooling phases.

Afterwards, the results of the thermographies are summed up. Each thermography was made by considering each combination of metal and PCM filler, in order to compare which one has a better thermal behaviour. Once the 48 thermographies were done, for each one were evaluated the seven core points of interest discussed in the previous chapter, to obtain the mean temperature histories during the testing phase. The temperature histories were plotted by considering the mean values of the cursors analysed during a single test, and the mean value between the three repetition tests with the three different cursor configurations. In this way, the results are less affected by the variability of the testing conditions. The eight mean temperature histories result of every tested condition were plotted, in Fig. 9 is shown different temperature histories by fixing the reticular structure and by changing the filler, whilst in Fig. 10 is fixed the filler used and changed the external compound structure. From the plots, it can be

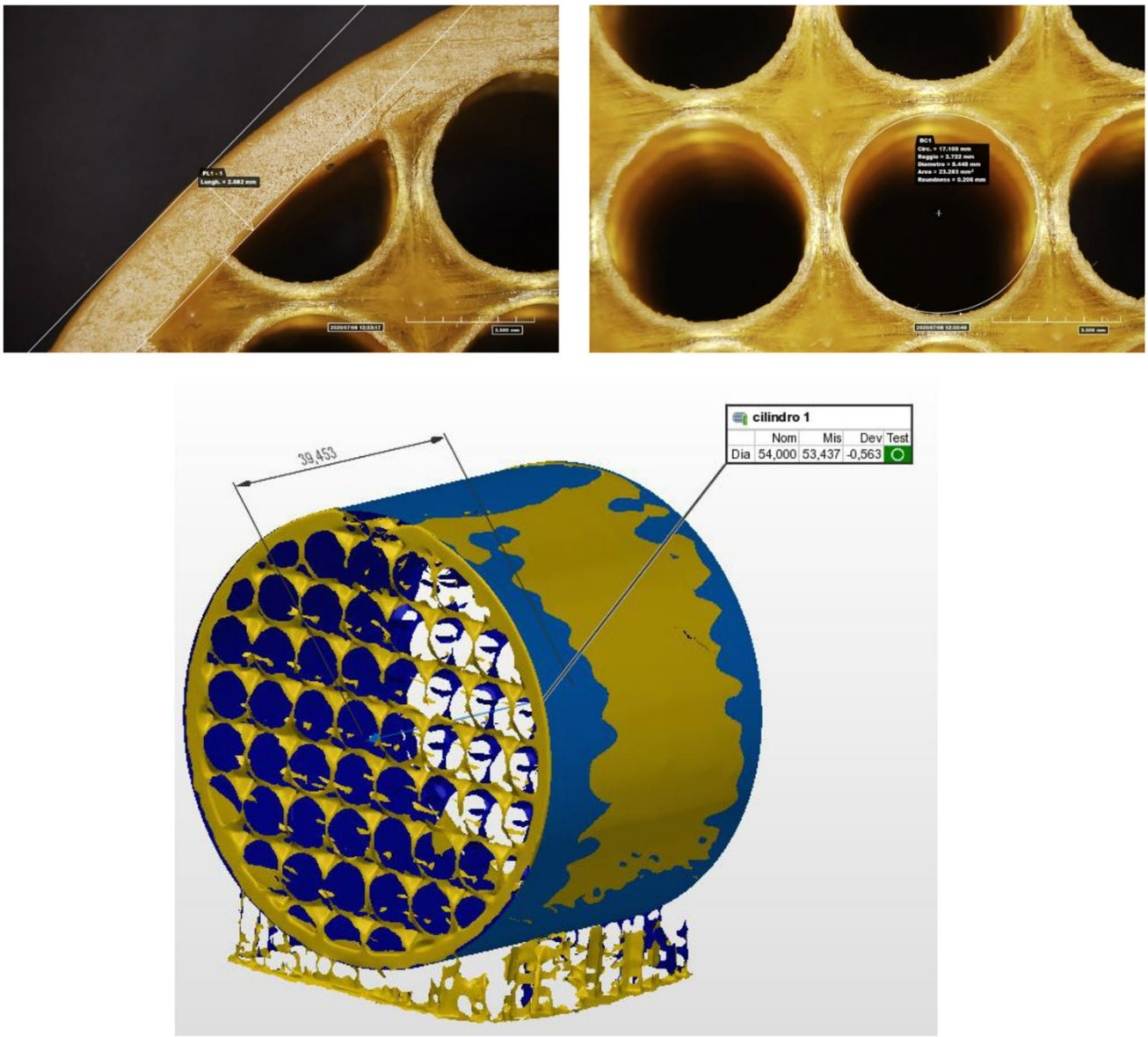

Fig. 7 Microscopical measurements on Ø 6.4 resin model realised

Table 2 Microscopical measurements of all 3D printed resin samples

	Axial length [mm]		Cylinder diameter [mm]		Cylinder thickness [mm]		Hole diameter [mm]		Thickness of the ligaments [mm]	
	Measured	Nominal	Measured	Nominal	Measured	Nominal	Measured	Nominal	Measured	Nominal
Al Ø3.2	39.78	40	53.84	54	2.02	2	5.38	5.4	1.02	1
Al Ø6.4	39.45	40	53.44	54	2.06	2	5.38	5.4	1.03	1
Cu Ø3.2	39.72	40	53.71	54	1.99	2	5.36	5.4	1.03	1
Cu Ø6.4	39.58	40	53.55	54	2.04	2	5.36	5.4	1.01	1

noted the different thermal behaviour of each bio-based filler and reticular structure. In each history there is an oscillating zone which happens due to the switch of the controller once the type K thermocouple connected in the middle of the samples reaches the 80 °C imposed temperature. The oscillation is ended once the controller is

Table 3 Weight of the samples realised through I-AM and PCM fillers in the reticular structure

	CAD model [g]	As built samples [g]	Pure temp 68 [g]	Crodatherm 60 [g]	Crodatherm 74 [g]	Crodatherm ME29P [g]
Al Ø3.2	48.56	49.29	54.78	54.39	53.44	23.04
Al Ø6.4	49.20	52.45	52.26	49.51	49.48	15.15
Cu Ø3.2	160.07	164.08	56.06	52.15	54.02	21.83
Cu Ø6.4	162.18	167.12	51.95	48.26	48.55	15.87

Fig. 8 Microscopical observations of the Ø 6.4 Cu sample filled with PCM Pure Temp 68 at different magnitudes

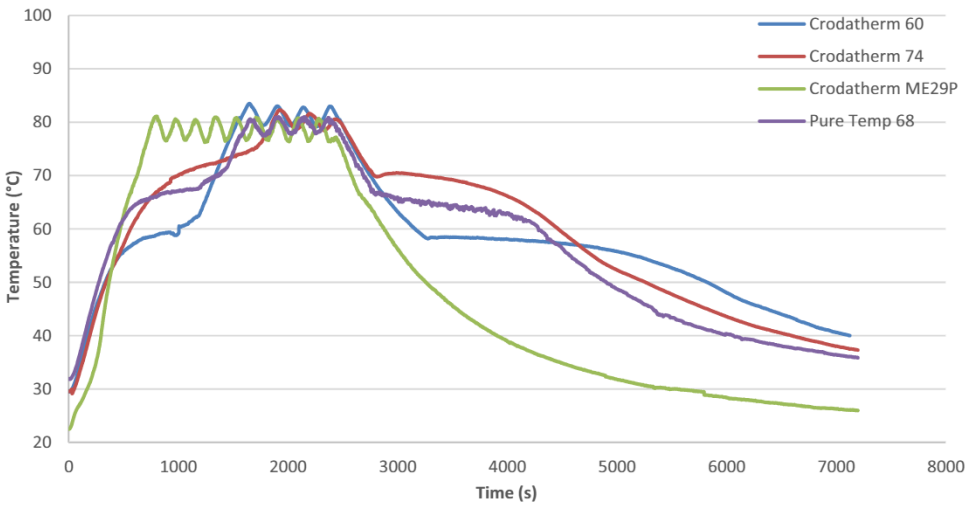

Fig. 9 Temperature histories of the different PCM fillers analysed in the Al Ø 6.4 sample

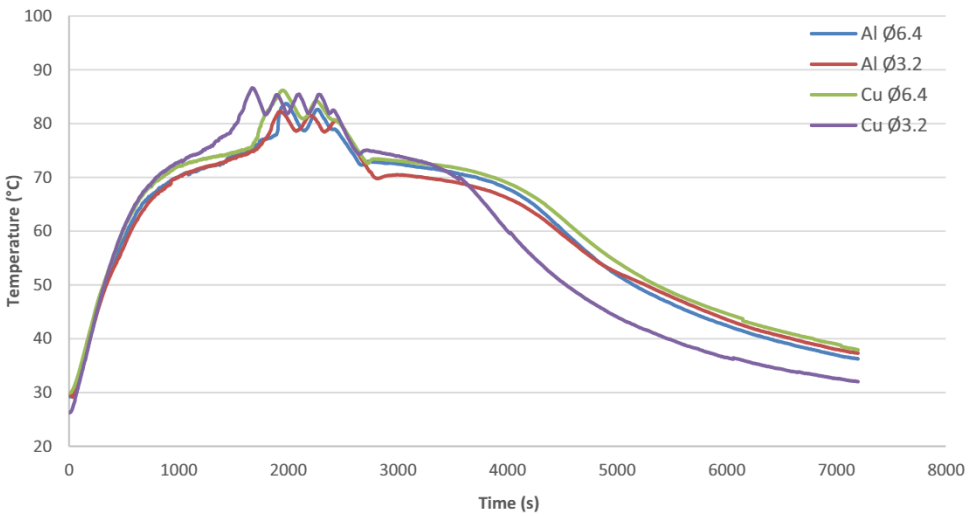

Fig. 10 Temperature histories of the different reticular structures considered filled with Crodatherm 74 PCM

shut down manually after 40 min and the heating phase is ended. The zones where the temperature is almost constant, are the ones where happens the phase change of the PCM filler. This phase is less evident for PCM filler Crodatherm ME29P, since it has a lower latent heat of fusion and solidification and the temperature of fusion/solidification is near the environmental one (28.8 °C). Due to these different proprieties, this filler is also the one that is heated/cooled before all the others, this behaviour can be noticed by the different slope of the temperature history and from the higher oscillation time after reaching the max temperature (80 °C). Moreover, it can be noted that the heating-up phase is always faster than the cooling one for each sample, which can be explained because there is a different mechanism of thermal exchange (conduction for heating, natural convection for cooling). From the plots in Fig. 9, is also evident the difference of behaviour of each typology of PCM by fixing the external compound structure due to their different thermal properties. At the end of the test, can be noted that the Crodatherm 60 is the one with the highest temperature, which means that releases the energy accumulated during the heating phase slowly than the others, which could be useful for applications that require a slower heat transfer. Plots in Fig. 10 show how the external reticular structure influences the Crodatherm 74 PCM thermal behaviour. It is notable that each structure reaches the first peak of the oscillation at different times, in particular the Cu Ø 3.2 structure it is the fastest one on both the heating and cooling phase since it exploits the uniform temperature distribution derived from the geometry, which allows a higher dispersion of PCM which is melted/cooled sooner. On the other hand, The Al Ø 6.4 is the one that heats up at the imposed temperature later than the others, this can be explained due to a non-uniform distribution of the thermal load and the lower thermal conductivity of the material. Besides the differences during the heating phase, the cooling behaviour for the other structures besides Cu Ø 3.2 is almost the same.

To put in evidence the aforementioned differences for all the 16 analysed configurations, from the temperature histories derived from thermographies, were calculated the parameters described in the second paragraph (T_h, T_{start}, T^c, T_{end}, t_h, t_c), knowing the thermal and geometrical proprieties of the system (m_v, m_f, λ_s, λ_f, c_s, c_l, c_m, T_{tf}, L) and by means of the Eqs. 1–8, were realised measurements of P^{h*}_{tot} and P^{c*}_{tot} for each geometry, material, and PCM during the two phases, as shown in Table 4. It is notable that the Cu Ø 3.2 structure is the one that leads to overall better storage of thermal energy during the heating phase, 10% more than the other ones if filled with the PCM Crodatherm 74, whilst the cooling release rate is maximised for the Cu Ø 6.4 sample. This increment of the energy absorbed and released by the copper structures can be attributed to the higher thermal conductivity of the base material, which leads to a more efficient heat transfer. However, a tradeoff between the highest thermal performance (reached with the copper structures) and a lower cost and weight of the heat exchanger (reached with the aluminium structures) must be considered during the design.

Table 4 P^{h*}_{tot} and P^{c*}_{tot} calculated from the results of thermographies

Reticular structure	Cell diameter [mm]	PCM filler	P^{h*}_{tot}[W/m]	P^{c*}_{tot}[W/m]
Al	Ø 3.2	Pure temp 68	278.707	94.489
		Crodatherm 60	269.604	91.742
		Crodatherm 74	253.422	92.738
		Crodatherm ME29P	233.964	33.560
	Ø 6.4	Pure Temp 68	296.756	101.562
		Crodatherm 60	311.694	96.669
		Crodatherm 74	264.608	102.723
		Crodatherm ME29P	223.739	45.484
Cu	Ø 3.2	Pure Temp 68	306.294	102.402
		Crodatherm 60	313.975	96.282
		Crodatherm 74	333.576	105.848
		Crodatherm ME29P	243.111	45.446
	Ø 6.4	Pure temp 68	297.027	108.896
		Crodatherm 60	293.737	97.241
		Crodatherm 74	291.011	107.383
		Crodatherm ME29P	288.192	49.275

To evaluate the influence of each parameter in thermal performances an ANoVA analysis was performed. The data showed in Table 4 were used to evaluate the differences for both the heating and cooling phases. In Table 5 is showed which effects are significant in terms of heating behaviour. On linear interaction, every factor does not affect the heating rate (P value < 0.05). During the heating process the influence of the the heating system is higher then that of the factors analysed, for this reason, none of their interactions are significant. The R^2 value shows that the model explains 89.94% of the variance in the heating phase, which indicates that the model fits the data with a little error of evaluation. Most of the VIFs are small, which indicates that the terms in the model are not correlated. On the contrary, the cooling behaviour for thermal storage and management is very interesting. In particular, the P value shows that on linear interaction, every factor is significant (P value < 0.05). In particular, Pareto charts showed in Fig. 11 put in evidence the big influence of PCM material factor compared to the others in both heating and cooling phase, even if during the former there is no valuable effect. Also, none of the two-way interactions are significant. The R^2 value shows that the model explains 99.90% of the variance in the cooling phase, which indicates that the model fits the data with an excellent

Table 5 Results from ANoVA analysis during the heating and cooling phases

Analysis of variance				
	Heating		Cooling	
Linear interactions	*F* value	*P* value	*F* value	*P* value
PCM	2.99	0.196	923.63	0
Cell diameter	0.10	0.771	39.17	0.008
Structural material	4.77	0.117	51.94	0.006
2-Way interactions				
PCM × Cell diameter	0.29	0.835	1.29	0.421
PCM × Structural material	0.52	0.697	2.3	0.255
Cell diameter × Structural material	0.67	0.472	7.98	0.066
	R-sq	R-sq(adj)	R-sq	R-sq(adj)
Model summary	89.94%	24.71%	99.90	99.48

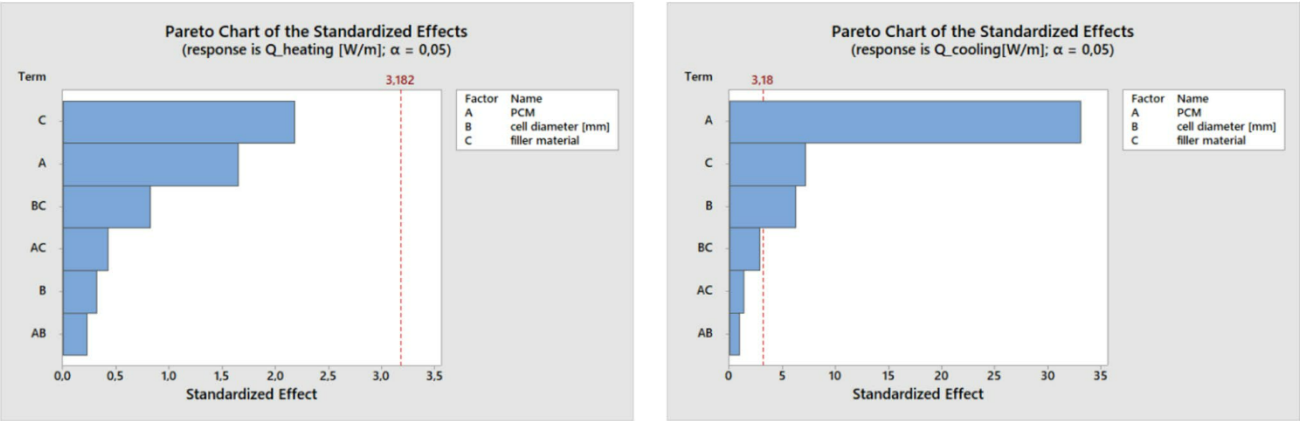

Fig. 11 Pareto chart of the standardised effects for the heating and cooling phases

fitting. Most of the VIFs are small, which indicates that the terms in the model are not correlated.

4 Conclusions

In this paper, compound structures filled with different typologies of PCM were realised and thermally characterised to design a modular prototype that can be used for thermal storage. In particular, 2 aluminium AC-44300 and 2 copper alloy structures with different pore dimensions (Ø 3.2; Ø 6.4) were produced through I-AM. The four chosen PCMs typology were melted and integrated into the reticular structures, for a total of 16 combinations of integrated structures.

The structures were tested and the results of each analysis performed can be summed up as follows:

- The resin models analysed and measured through 3D laser scanner ZG Technology – Atlascan showed differences of 0.2–0.5 mm on diameter and axial length, and 0.01–0.05 mm for the thickness of the ligaments and the diameters of the holes, in accordance with the tolerance generated with the SLA process.
- The adhesion of the PCM with the metal matrix was confirmed by the HIROX RH2000 images and is an extremely favourable feature in the management of thermal energy.
- 16 thermographies repeated 3 times were done to evaluate the thermal performance of each configuration, in order to obtain the mean temperature histories during the testing phase. The temperature histories showed clearly the different behaviour of the different typologies of PCMs due to the different latent heat of melting/solidification and phase transition temperature.
- From the thermographies and data from plots of temperature history, were calculated P_{tot}^{h*} and P_{tot}^{c*} which showed an increase of 10% of the thermal storage performance of the copper structures with the PCM filler Crodatherm 74 and Pure temp 68, even if the weight

and cost of the structure are higher than the aluminium ones.

- The ANoVA analysis showed that during the heating process is predominant the heating system and none of the interactions between the analysed parameters are significant. On the contrary, the cooling behaviour for thermal storage and management put in evidence the big influence of PCM material factor compared to the others, with every linear interaction significant.

Author's contributions All the authors contributed equally to the various aspects of this work: DA: methodology, formal analysis, software, writing-original draft, investigation; EM: formal analysis, investigation, writing-original draft, methodology, software, investigation; NU: conceptualization, methodology, validation, formal analysis; VT: validation, conceptualization, methodology, formal analysis.

Funding Open access funding provided by Universita degli Studi della Campania Luigi Vanvitelli within the CRUI-CARE Agreement. This study was partially supported by an academic grant (Funding program VALERE assigned to Emanuele Mingione) from the University of Campania Luigi Vanvitelli. The authors are particularly grateful to the Interuniversity Research Centre CIRTIBS for the equipment and the financial support to develop the present research work.

Data Availability The processed data generated and analysed during the current study are available from the corresponding author on reasonable request.

Declarations

Conflict of interest The authors declare that they have no known competing financial interests or personal relationships that could have appeared to influence the work reported in this paper.

Code availability Not applicable.

Ethical approval Not applicable.

Consent to participate Not applicable.

Consent for publication Not applicable.

References

1. O'Shaughnessy E, Heeter J, Shah C, Koebrich S (2021) Corporate acceleration of the renewable energy transition and implications for electric grids. Renew Sustain Energy Rev. 146:111160
2. Cole W, Gates N, Mai T (2021) Exploring the cost implications of increased renewable energy for the U.S. power system. Electr J 34(5)
3. Smirnova E, Kot S, Kolpak E, Shestak V (2021) Governmental support and renewable energy production: a cross-country review. Energy. https://doi.org/10.1016/j.energy.2021.120903
4. Esen H, Esen M, Ozsolak O (2017) Modelling and experimental performance analysis of solar-assisted ground source heat pump system. J Exp Theor Artif Intell 29(1):1–17
5. Esen M, Yuksel T (2013) Experimental evaluation of using various renewable energy sources for heating a greenhouse. Energy Build 65:340–351
6. Liu Y, Zhang Q, Xu M, Yuan H, Chen Y, Zhang J et al (2019) Novel and efficient synthesis of Ag-ZnO nanoparticles for the sunlight-induced photocatalytic degradation. Appl Surf Sci 476:632–640. https://doi.org/10.1016/j.apsusc.2019.01.137
7. Strušnik D, Brandl D, Schober H, Ferčec J, Avsec J (2021) A simulation model of the application of the solar STAF panel heat transfer and noise reduction with and without a transparent plate: a renewable energy review. Renew Sustain Energy Rev 134
8. Abu-Hamdeh NH, Khorasani S, Oztop HF, Alnefaie KA (2021) Numerical analysis on heat transfer of a pyramid-shaped photovoltaic panel. J Therm Anal Calorim
9. Pawar V, Sobhansarbandi S (2021) Design optimization and heat transfer enhancement of energy storage based solar thermal collector. Sustain Energy Technol Assessments 46
10. Chen X, Wang D, Wang T, Yang Z, Zou X, Wang P et al (2019) Enhanced photoresponsivity of a GaAs nanowire metal-semiconductor-metal photodetector by adjusting the fermi level. ACS Appl Mater Interfaces 11:33188–33193
11. Mehdizadeh Youshanlouei M, Yekani Motlagh S, Soltanipour H (2021) The effect of magnetic field on the performance improvement of a conventional solar still: a numerical study. Environ Sci Pollut Res
12. Jia L, Liu B, Zhao Y, Chen W, Mou D, Fu J et al (2020) Structure design of MoS2@Mo2C on nitrogen-doped carbon for enhanced alkaline hydrogen evolution reaction. J Mater Sci 55:16197–16210
13. Wei Z, Chen W, Wang Z, Li N, Zhang P, Zhang M et al (2020) High-temperature persistent luminescence and visual dual-emitting optical temperature sensing in self-activated CaNb2O6: Tb3+ phosphor. J Am Ceram Soc n.d
14. Cui D, Li J, Zhang X, Zhang L, Chang H, Wang Q (2021) Pyrolysis temperature effect on compositions of basic nitrogen species in Huadian shale oil using positiveion ESI FT-ICR MS and GC-NCD. J Anal Appl Pyrolysis 153:104980
15. Hasnain SM (1998) Review on sustainable thermal energy storage technologies, part I: heat storage materials and techniques. Energy Convers Manag
16. Agyenim F, Hewitt N, Eames P, Smyth M (2010) A review of materials, heat transfer and phase change problem formulation for latent heat thermal energy storage systems (LHTESS). Renew Sustain Energy Rev 14:615–628
17. Khadiran T, Hussein MZ, Zainal Z, Rusli R (2016) Advanced energy storage materials for building applications and their thermal performance characterization: a review. Renew Sustain Energy Rev 57:916–928
18. Ghalambaz M, Doostani A, Izadpanahi E, Chamkha AJ (2017) Phase-change heat transfer in a cavity heated from below : the

effect of utilizing single or hybrid nanoparticles as additives. J Taiwan Inst Chem Eng 1–12
19. Cao X, Yuan Y, Xiang B, Sun L, Xingxing Z (2018) Numerical investigation on optimal number of longitudinal fins in horizontal annular phase change unit at different wall temperatures. Energy Build 158:384–392
20. Joneidi MH, Rahimi M, Pakrouh R, Bahrampoury R (2020) Experimental analysis of transient melting process in a horizontal cavity with different configurations of fins. Renew Energy 145:2451–2462
21. Acır A, Emin Canlı M (2018) Investigation of fin application effects on melting time in a latent thermal energy storage system with phase change material (PCM). Appl Therm Eng 144:1071–1080
22. P´erez-Lombard L, Ortiz J, Pout C (2008) A review on buildings energy consumption information. Energy Build 40(3):394–398
23. Esmaeilzadeh A, Zakerzadeh MR, Koma AY (2018) The comparison of some advanced control methods for energy optimization and comfort management in buildings. Sustain Cities Soc 43:601–623
24. GhaffarianHoseini A, Dahlan ND, Berardi U, GhaffarianHoseini A, Makaremi N, GhaffarianHoseini M (2013) Sustainable energy performances of green buildings: a review of current theories, implementations and challenges. Renew Sustain Energy Rev 25:1–17
25. Hassan MA, Shebl SS, Ibrahim EA, Aglan HA (2011) Modeling and validation of the thermal performance of an affordable, energy efficient, healthy dwelling unit. Build Simul 4(3):255–262
26. Wi S, Chang SJ, Kim S (2020) Improvement of thermal inertia effect in buildings using shape stabilized PCM wallboard based on the enthalpy-temperature function. Sustain Cities Soc 56:102067
27. Meggers F, Leibundgut H, Kennedy S, Qin M, Schlaich M, Sobek W et al (2012) Reduce CO2 from buildings with technology to zero emissions. Sustain Cities Soc 2(1):29–36
28. Stritih U, Tyagi VV, Stropnik R, Paksoy H, Haghighat F, Joybari MM (2018) Integration of passive PCM technologies for net-zero energy buildings. Sustain Cities Soc 41:286–295
29. Almonti D, Ucciardello N (2019) Design and thermal comparison of random structures realized by indirect additive manufacturing. Materials 2261
30. Almonti D, Baiocco G, Tagliaferri V, Ucciardello N (2020) Design and mechanical characterization of voronoi structures manufactured by indirect additive manufacturing. Materials 13:1085
31. Almonti D, Baiocco G, Mingione E, Ucciardello N (2020) Evaluation of the effects of the metal foams geometrical features on thermal and fluid-dynamical behavior in forced convection. Int Journ Adva Manuf Technol 111:1157–1172
32. Bi Z, Zhang W (2001) Modularity technology in manufacturing: taxonomy and issues. Int J Adv Manuf Technol 18:381–390
33. Mandolfino C, Lertora E, Genna S, Leone C, Gambaro C (2015) Effect of laser and plasma surface cleaning on mechanical properties of adhesive bonded joints. Procedia CIRP 33:458
34. D'Addona DM, Genna S, Giordano A, Leone C, Matarazzo D, Nele L (2015) Laser ablation of primer during the welding process of iron plate for shipbuilding industry. Procedia CIRP 33:464
35. Genna S, Lambiase F, Leone C (2018) Effect of laser cleaning in laser assisted joining of CFRP and PC sheets. Comp Part B Eng 145:206